# Effects of hardware design and operation conditions on PEM fuel cell water flooding

Zhang, Jianlu; Li, Hui; Shi, Zheng; Zhang, Jiujun



**Publisher's version / Version de l'éditeur:**
http://dx.doi.org/10.1080/15435075.2010.515185
*International Journal of Green Energy, 7, 5, pp. 461-474, 2010-10-13*

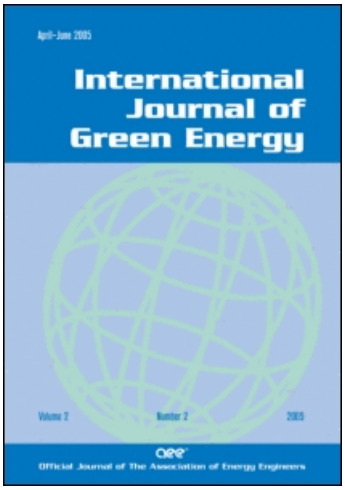


**International Journal of Green Energy**
Publication details, including instructions for authors and subscription information:
http://www.informaworld.com/smpp/title~content=t713597260

# Effects of Hardware Design and Operation Conditions on PEM Fuel Cell Water Flooding

Jianlu Zhang[a]; Hui Li[a]; Zheng Shi[a]; Jiujun Zhang[a]
[a] Institute for Fuel Cell Innovation, National Research Council of Canada, Vancouver, B.C., Canada

Online publication date: 13 October 2010

**To cite this Article** Zhang, Jianlu , Li, Hui , Shi, Zheng and Zhang, Jiujun(2010) 'Effects of Hardware Design and Operation Conditions on PEM Fuel Cell Water Flooding', International Journal of Green Energy, 7: 5, 461 — 474
**To link to this Article: DOI:** 10.1080/15435075.2010.515185
**URL:** http://dx.doi.org/10.1080/15435075.2010.515185

*International Journal of Green Energy*, 7: 461–474, 2010

ISSN: 1543-5075 print / 1543-5083 online
DOI: 10.1080/15435075.2010.515185

Taylor & Francis
Taylor & Francis Group

# EFFECTS OF HARDWARE DESIGN AND OPERATION CONDITIONS ON PEM FUEL CELL WATER FLOODING

**Jianlu Zhang, Hui Li, Zheng Shi, and Jiujun Zhang**

*Institute for Fuel Cell Innovation, National Research Council of Canada, Vancouver, B.C., Canada, V6T 1W5*

***In this paper, membrane electrode assemblies were constructed using catalyst-coated membranes to investigate proton-exchange membrane fuel cell water flooding. Two major fuel cell hardware variations, namely flowfield design and Teflon loading of the gas diffusion layer (GDL), were tested to explore their effects on water flooding. A flowfield with triple serpentine flow channels showed heavier water flooding than that with single serpentine flow channels. Increasing the Teflon loading in the GDL reduced water flooding effectively. Several fuel cell operating conditions, including air stoichiometry, current density, relative humidity (RH), backpressure, and temperature, were also tested to identify their effects on water flooding. It was observed that the water flooding severity increased with decreasing air stoichiometry, as well as with increasing temperature, RH, backpressure, and current density. Among these operation conditions, air stoichiometry (or air flow rate) and RH played more important roles in reducing water flooding.***

**Keywords:** ***AC impedance spectroscopy (EIS); Flow field; Mass transfer; Operating conditions; Proton-exchange membrane (PEM) fuel cells; Teflon (PTFE) loading; Water flooding***



## INTRODUCTION

Proton-exchange membrane or polymer electrolyte membrane (PEM) fuel cells are considered promising energy converters due to their high power density, high energy conversion efficiency, quick start-up, and environmental friendliness (Haile et al. 2001; Steele and Heinzel 2001). However, obstacles to their commercialization still exist, notably issues of durability/reliability and high cost. With respect to the first issue, slow mass transfer of oxidant (e.g., oxygen) and insufficient removal of the product (e.g., water) at cathode have been identified as the major contributors to the low durability. For example, if the water produced at cathode could not be effectively removed, "water flooding" will occur, resulting in a significant performance degradation including fuel cell voltage fluctuation (Li et al. 2008). Therefore, water management at fuel cell cathode has been recognized as a key approach for reducing degradation and improving performance.

Address correspondence to Jiujun Zhang, Institute for Fuel Cell Innovation, National Research Council of Canada, Vancouver, B.C., Canada, V6T 1W5. E-mail: jiujun.zhang@nrc.gc.ca

At a PEM fuel cell cathode, the water comes primarily from three sources: (1) the electrochemical oxygen reduction reaction (ORR) (half-cell reaction: $O_2 + 4H^+ + 4e^- \rightarrow 2H_2O$) to produce water; (2) gas humidification; and (3) water dragged electro-osmotically from the anode side. When liquid water accumulates at the cathode, water droplets form and block the flowfield channels and/or pores in the gas diffusion layer (GDL) and/or catalyst layer, thereby hinder the transport of reactant species. As a result, fuel cell performance deceased suddenly and dramatically, but recovers if the water droplets are removed. This phenomenon is usually called "water flooding."

Water flooding, a significant problem in PEM fuel cells, is a complex phenomenon of interrelated factors. The severity of water flooding depends on fuel cell design, flowfield patterns, and operating conditions (Wang et al. 2008; Weng et al. 2007). Water flooding usually happens at high current densities, although it also occurs at lower current densities if the gas stoichiometry is small (He et al. 2003; Larminie and Dicks 2001). In recent years, water flooding has garnered significant attention, having been recognized as a primary degradation mode. In our pervious review paper (Li et al. 2008), we examined the water flooding issue and its effects on fuel cell performance.

In various efforts to develop mitigation strategies for water flooding, researchers have carried out numerous studies using numerical simulations and predictions (modeling) (Le and Zhou 2009; McKay et al. 2008; Meng and Wang 2005; Patel et al. 2008; Wang et al. 2001; Yuan and Sundén 2004), as well as experimental investigation and diagnosis (Canut et al. 2006; Ihonen et al. 2004; Spernjak et al. 2007; Weng et al. 2007). Fundamental modeling that addresses water flooding through a two-phase flow model has developed rapidly, and is demonstrably useful in understanding both the importance of water management and the sensitivity of water flooding to fuel cell operating conditions and components. Direct visualization (Hakenjos et al. 2004; Spernjak et al. 2007; Tüber et al. 2003; Weng et al. 2007; Yang et al. 2004) and pressure drop measurement (Barbir et al. 2005; He et al. 2003; Park and Caton 2008; Tüber et al. 2003) methods have also been well developed, especially for qualitatively investigating water flooding. With respect to the experimental approaches, considerable effort has been put into mitigating water flooding. Tactics include changing flowfield designs, treating the GDL hydrophobically with Teflon (PTFE), applying a micro-porous layer (MPL) between the gas diffusion media (e.g., carbon paper) and the catalyst layer, changing fuel cell orientation with respect to gravity (Benziger et al. 2007), and optimizing fuel cell operating conditions. Each of these strategies seems very successful for flooding mitigation in a PEM fuel cell.

For this paper, water flooding in a PEM fuel cell was recorded under various experimental conditions. The effects of operating conditions (temperature, relative humidity, air stoichiometry, and backpressure), flowfield channel design, and Teflon loading on the gas diffusion layer were systematically studied. In addition, the severity of water flooding in fuel cells was defined and the severities under different conditions were compared during lifetime testing. AC impedance was also used to diagnose water flooding during fuel cell operation.

## EXPERIMENTAL DETAILS

The membrane electrode assemblies (MEAs) with an active area of 50 $cm^2$ were prepared by compressing, in each case, two GDLs against one catalyst coated membrane (CCM). The CCMs were made of Nafion 211 membrane with 0.4 $mg/cm^2$ Pt loading on both anode and cathode sides. The GDLs consisted of carbon papers impregnated

by both Teflon (PTFE) (20 wt% and/or 5 wt%) and carbon black. Single cell hardware with end plates (50 $cm^2$ CH-50) and the heating cartridges were purchased from Teledyne Technologies Inc. The flowfield plates were designed and fabricated in-house using both triple and single serpentine flow channels, with a channel depth of 1.0 mm, a land width of 1.0 mm, and variable channel widths.

A Fideris fuel cell test station controlled with FC Power software was used for fuel cell data collection. In all fuel cell tests, hydrogen and air were used as fuel and oxidant, respectively, and their particular mass flow controllers were used to manage their flow rates. Before being fed into the anode and cathode, $H_2$ and air were humidified by passing through their designated humidifiers at the temperature corresponding to the required relative humidity (RH). The stoichiometry of $H_2$ ($H_{2,ST}$) was controlled at 1.5, and the air stoichiometries ($Air_{st}$) were controlled at various selected values. Two pressure sensors were installed, at the fuel cell inlet and outlet on the cathode side, to measure the pressure drop across the flow channel. Polarization data were collected and the cell voltage under each current density was recorded after the reading stabilized. During all tests, the backpressures and RHs for the anode and cathode sides were kept the same. In experiments studying the RH effect, the RH at anode side was controlled at 100%, while the RH was variously adjusted to the required experimental levels at the cathode side.

A Solartron 1252 FRA was used for AC impedance measurements, taken in the frequency range of 5000 to 0.01 Hz using a method described in our previous paper (Tang et al. 2006). AC impedance was employed to obtain mass transfer resistances for the fuel cell reactions.



## RESULTS AND DISCUSSION

### Water Flooding Observation and Description

Figure 1 shows a typical fuel cell voltage–time curve at a current density of 0.5 $A/cm^2$. Many sharp downward peaks are observable on the curve, occurring randomly since the time intervals between two adjacent peaks are not the same. Cathode water flooding caused these downward peaks, the formation of which can be conceptualized as follows. When water droplets that have formed near or on the gas diffusion layer surface cannot be effectively removed by the air flowing within the flowfield channels, they block the access of reactant ($O_2$) to the reaction sites, leading to a rapid drop in the cell voltage when the majority of the GDL surface is covered by these water droplets. Because the droplets block the air flow through the flowfield channels, the pressure drop between the gas inlet and outlet increases. When this pressure differential reaches a high enough value, it blows out the water, and the reaction sites blocked by these water droplets are released, resulting in a swift voltage recovery. This may be the major process contributing to the water flooding, but it is not the only one. Other water transfer processes occurring inside the catalyst layer and GDL might also contribute to water flooding. However, in order to quantitatively compare the severity of water flooding under different conditions, in this paper we introduce a function $\Psi_{wf}$, identified as the water flooding severity. Here $\Psi_{wf}$ is defined as a product of $N_{wf}$ and $\Delta V_{wf}^{ave}$:

$$\Psi_{wf} = N_{wf} \Delta V_{wf}^{ave}, \tag{1}$$

where $N_{wf}$ is the number of water flooding downward peaks in one minute, expressed as $min^{-1}$. For example, in Figure 1, 15 peaks occur within 150 minutes; therefore, the $N_{wf}$

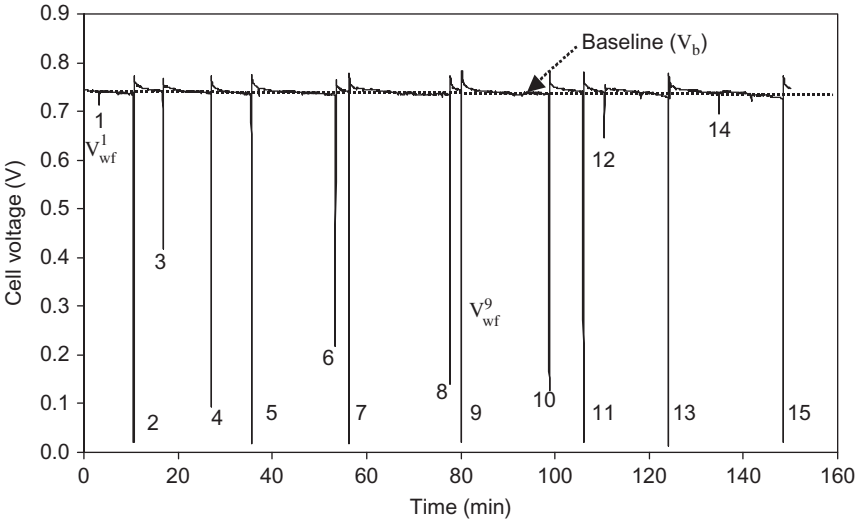


**Figure 1** Fuel cell voltage as a function of time at a current density of 0.5 A/cm$^2$. MEA area: 50 cm$^2$. The fuel cell flowfield design had triple serpentine flow channels. The depth and width of the channel were both 1.0 mm. GDL Teflon loading: 5 wt%. Operating conditions: 80°C, 100% RH, 3.04 atm, $H_{2,ST} = 1.5$, and $Air_{ST} = 2.0$.



value should be 15/150, which is 0.1 min$^{-1}$. In Equation (1), $\Delta V^{ave}_{wf}$ is the average cell voltage drop caused by water flooding over a certain operating time period, expressed in mV. As marked in Figure 1, $V_b$ is the baseline cell voltage and $V^i_{wf}$is the height of downward peaks caused by water flooding, in mV. Equation (2) can be used to express $\Delta V^{ave}_{wf}$:

$$\Delta V^{ave}_{wf} = \frac{1}{n}\sum_{i=1}^{n}\left(V_b - V^i_{wf}\right), \tag{2}$$

where $n$ is the total number of water flooding peaks over the whole testing period. For example, in the case of Figure 1, $n$ equals 15.

## Effect of Air Stoichiometry (or Air Flow Rate) on Water Flooding

The effect of air stoichiometry or air flow rate on water flooding was also tested using several air stoichiometries. Figure 2 shows two typical curves of cell voltage versus time, obtained when fuel cell was operated at a current density of 0.5 A/cm$^2$ for 150 minutes. It can be seen that as air stoichiometry increased from 2.0 to 3.5, both the number and the voltage magnitude of downward peaks decreased significantly. This result further confirms that the downward peaks on the voltage–time curves are caused by inefficient water removal. It is understandable that at a higher air stoichiometry, which corresponds to a higher air flow rate, the removal of water drops near/on the GDL surface will occur more rapidly, leading to less water flooding. In addition, at a high air flow rate, the pressure drop between the gas inlet and outlet will be larger, making water removal easier.

The results presented in Figure 2 demonstrate that increasing air stoichiometry or flow rate can effectively reduce water flooding. However, in practical fuel cell operation,

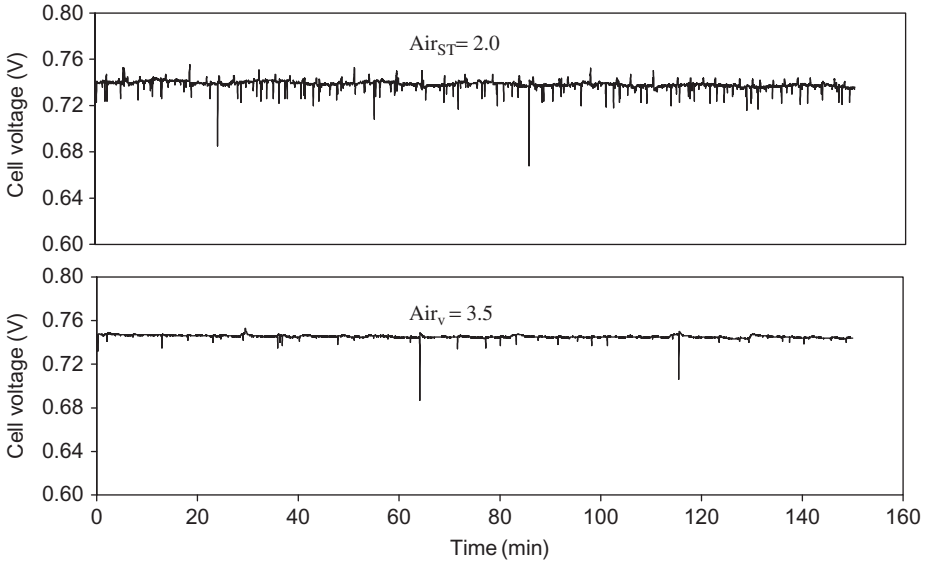


**Figure 2** Fuel cell voltage as a function of time at two different air stoichiometries. MEA area: 50 cm$^2$. GDL Teflon loading: 20 wt%. The fuel cell flowfield design had triple serpentine flow channels. The depth and width of the channel were both 1.0 mm. Operating conditions: current density of 0.5 A/cm$^2$; 80°C; 100% RH; 3.04 atm; $H_{2,ST} = 1.5$; and $Air_{ST}$ as marked in the figure.

increasing the air stoichiometry will also increase system's parasitic loss. Therefore, optimization of air stoichiometry is also necessary when using this strategy to reduce water flooding.

## Effect of Current Density on the Water Flooding

In order to observe the effect of current density on the water flooding, the cell voltage–time curves were also recorded at three different current densities, 0.2, 0.5, and 1.0 A/cm$^2$, as shown in Figure 3. The baseline voltage ($V_b$) in Figure 3 should represent the steady-state performance at its corresponding current density. The fuel cell showed fairly high performance, achieving voltages of 0.82, 0.74, and 0.63 V at current densities of 0.2, 0.5, and 1.0 A/cm$^2$, respectively.

In terms of water flooding, downward voltage peaks can be observed in Figure 3 at all three current densities. At a low current density such as 0.2 A/cm$^2$, just a few small peaks appear on the voltage curve, indicating only occasional water flooding. When the current density increases from 0.2 to 0.5 A/cm$^2$, the peaks occur more frequently, indicating more severe water flooding. This would have occurred because more water is produced at higher current densities. However, when the current density went up to 1.0 A/cm$^2$, the flooding situation seems to have improved. In order to quantitatively compare the severity of water flooding under different conditions, the water flooding severity ($\Psi_{wf}$) was calculated according to Equation (1), based on the data shown in Figure 3. As listed in Table 1, when the current density rises from 0.2 to 0.5 A/cm$^2$, the value of $\Psi_{wf}$ increases from 1.7 to 22.2 mV/min, while when the current density increases further to 1.0 A/cm$^2$, the value of $\Psi_{wf}$ drops to 20.3 mV/min. This can be explained in terms of water generation,

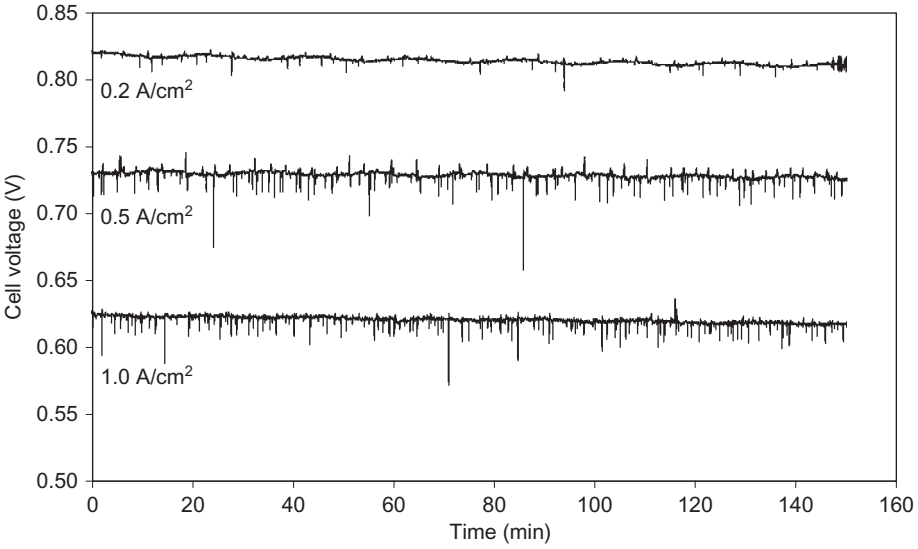


**Figure 3** Fuel cell performance as a function of time at three different current densities. MEA area: 50 $cm^2$. GDL Teflon loading: 20 wt%. The fuel cell had a flowfield design with triple serpentine flow channels. The depth and width of the channel were both 1.0 mm. Operating conditions: 80°C, 100% RH, 3.04 atm, $H_{2,ST} = 1.5$, $Air_{ST} = 2.0$.

**Table 1** Water flooding severity at three different current densities (data from Figure 3).

| Current density ($A/cm^2$) | $N_{wf}$ ($min^{-1}$) | $\Delta V_{wf}^{ave}$ (mV) | $\Psi_{wf}$ (mV/min) |
|---|---|---|---|
| 0.2 | 0.17 | 9.5 | 1.7 |
| 0.5 | 0.73 | 30.3 | 22.2 |
| 1.0 | 1.03 | 19.7 | 20.3 |

gas flow rate, and cathodic pressure drop between the fuel cell inlet and outlet. When the current density was increased from 0.5 to 1.0 $A/cm^2$, more water was generated by the electrochemical reaction of oxygen reduction; however, the flow rate of air also would have increased if the air stoichiometry remained fixed. In this case, the water would have been more easily purged from the fuel cell by a higher gas flow rate, reflected by a higher $N_{wf}$ value (i.e., an increased number of water flooding downward peaks) and lower $\Delta V_{wf}^{ave}$ value (i.e., a decreased average cell voltage drop). In addition, the pressure drop between the fuel cell inlet and outlet rose with increasing current density. As shown in Figure 4, when the current density increased from 0.5 to 1.0 $A/cm^2$, the pressure drop rose from 0.086 to 0.17 atm. A greater pressure drop is definitely helpful for removing liquid water from the fuel cell. The trade-off between water generation and water removal thus results in slightly less severe water flooding at 1.0 than at 0.5 $A/cm^2$.

## RH Effect on Water Flooding

It was also observed that RH could strongly affect water flooding. As shown in Table 2, the water flooding becomes less acute with decreasing RH. For example, from

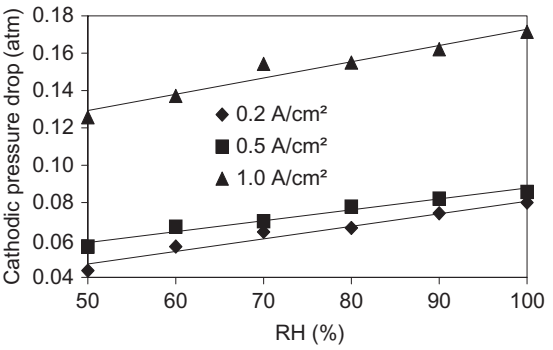


**Figure 4** Cathodic pressure drop as a function of relative humidity at three different current densities. MEA area: 50 $cm^2$. The fuel cell flowfield design had triple serpentine flow channels. The depth and width of the channel were both 1.0 mm. Operating conditions: 80°C, 100% RH, 3.04 atm, $H_{2,ST} = 1.5$, $Air_{ST} = 2.0$.

**Table 2** Water flooding severity at 0.5 $A/cm^2$ and different relative humidities with triple serpentine flow channels on flowfield plates.

| RH (%) | $N_{wf}$ ($min^{-1}$) | $\Delta V_{wf}^{ave}$ (mV) | $\Psi_{wf}$ (mV/min) |
|---|---|---|---|
| 100 | 0.73 | 30.3 | 22.2 |
| 80 | 0.60 | 36.3 | 21.8 |
| 50 | 0.44 | 35.0 | 15.4 |
| 35 | 0.02 | 10.0 | 0.2 |

*Note*. The depth and width of channel were both 1.0 mm. MEA: 50 $cm^2$. GDL Teflon loading: 20 wt%. Operating conditions: 80°C, 3.04 atm, $H_{2,ST} = 1.5$, $Air_{ST} = 2.0$.



100% to 50% RH, the water flooding severity gradually decreased, and at 35% RH, almost no water flooding could be observed. It is understandable from a thermodynamic point of view that if the inlet air has a lower relative humidity, water droplets near/on the GDL surface will more easily evaporate, reducing the extent of water flooding; at 35% RH in particular, the water removal became even easier. However, as shown in Figure 4, RH can also affect the cathode pressure drop between the fuel cell inlet and outlet, i.e., the cathode pressure drop increases with increasing RH. A greater cathode pressure drop at higher RH should be beneficial for water removal, suggesting less severe water flooding will occur at a higher RH. Therefore, there is a trade-off between the thermodynamic evaporation effect and the pressure drop effect. The results shown in Table 2 suggest that the water flooding reduction caused by thermodynamic evaporation may play a larger role than the water flooding increase caused by a drop in pressure, leading to a net water flooding reduction effect as RH decreases.

The water flooding phenomenon can also be detected using AC impedance measurements. Obviously, water flooding will slow down the mass transfer of $O_2$, which will be reflected by an increase in mass transfer resistance ($R_{mt}$) in the equivalent circuit of the cathode reaction process (Canut et al. 2006; Tang et al. 2006). As shown in Figure 5, the mass transfer resistances obtained based on AC impedance data increase with rising RH, indicating that at a higher RH water flooding has a more severe effect on the mass transfer process. The results in Table 2 suggest that running a fuel cell at a lower RH would be beneficial to reduce water flooding. However, under real-world fuel cell operating conditions,

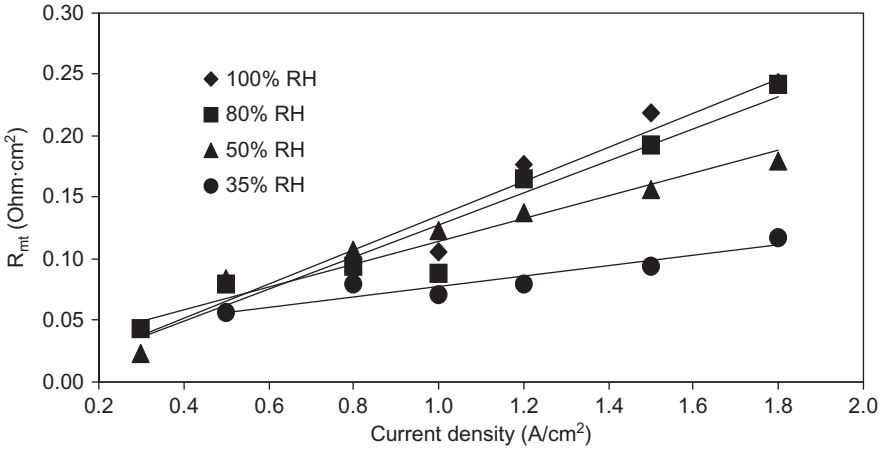


**Figure 5** Mass transfer resistances as a function of current density at different RHs with triple serpentine flow channels on flowfield plates. The depth and width of the channel were both 1.0 mm. MEA: 50 $cm^2$. GDL Teflon loading: 20 wt%. Current density: 0.5 $A/cm^2$. Operating conditions: 80°C, 3.04 atm, $H_{2,ST} = 1.5$, $Air_{ST} = 2.0$.



decreasing the RH will reduce fuel cell performance. Therefore, when trying to reduce water flooding, optimization of RH is also necessary.

## Backpressure Effect on Water Flooding

As presented in Table 3, the water flooding severity declined with decreasing backpressure. Because the fuel cell was operated at a fixed current density (0.5 $A/cm^2$) and a fixed air stoichiometry (2.0), the air volumetric flow rate at a higher backpressure would have been smaller than that at a lower backpressure. The larger air flow rate at a lower backpressure would have aided in water removal, resulting in a less water flooding. In addition, a higher cathode pressure drop at lower pressure, as shown in Figure 6, is helpful for water removal, as previously discussed.

## Temperature Effect on Water Flooding

Table 4 presents water flooding severities at different temperatures. It can be seen that as the temperature increased from 40°C to 80°C, the frequency of water flooding rose significantly (from 0.15 to 0.73 $min^{-1}$), although the average cell voltage change improved,

**Table 3** Water flooding severity at 0.5 $A/cm^2$ and different backpressures with triple serpentine flow channels on flowfield plates.

| Backpressure (atm) | $N_{wf}$ ($min^{-1}$) | $\Delta V_{wf}^{ave}$ (mV) | $\Psi_{wf}$ (mV/min) |
|---|---|---|---|
| 3.04 | 0.73 | 30.3 | 22.2 |
| 2.02 | 0.65 | 14.6 | 9.5 |
| 1.00 | 0.08 | 7.0 | 0.6 |

*Note*. The depth and width of channel were both 1.0 mm. MEA: 50 $cm^2$. GDL Teflon loading: 20 wt%. Operating conditions: 80°C, 100% RH, $H_{2,ST} = 1.5$, $Air_{ST} = 2.0$.

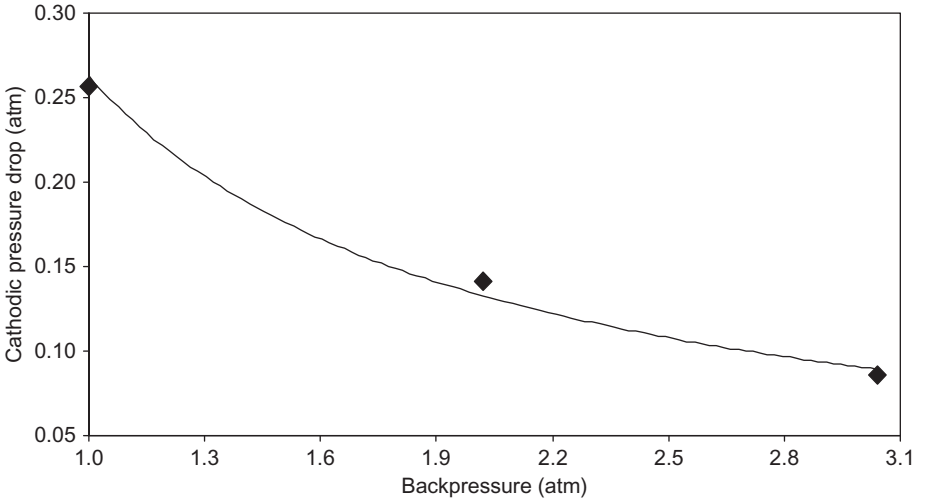


**Figure 6** Fuel cell cathode pressure drop as a function of backpressure at a current density of 0.5 A/cm$^2$ with triple serpentine flow channels on flowfield plates. The depth and width of the channel were both 1.0 mm. MEA: 50 cm$^2$. GDL Teflon loading: 20 wt%. Operating conditions: 80°C, 100% RH, $H_{2,ST} = 1.5$, $Air_{ST} = 2.0$.

**Table 4** Water flooding severity at 0.5 A/cm$^2$ and different temperatures.

| Temperature (°C) | $N_{wf}$ (min$^{-1}$) | $\Delta V_{wf}^{ave}$ (mV) | $\Psi_{wf}$ (mV/min) |
|---|---|---|---|
| 80 | 0.73 | 30.3 | 22.2 |
| 60 | 0.35 | 41.9 | 14.8 |
| 40 | 0.15 | 47.8 | 7.0 |

*Note*. Fuel cell flowfield design has triple serpentine flow channels. The depth and width of channel were both 1.0 mm. MEA area: 50 cm$^2$. GDL Teflon loading: 20 wt%. Operating conditions: 100% RH, 3.04 atm, $H_{2,ST} = 1.5$, $Air_{ST} = 2.0$.

going from 47.8 to 30.3 mV. The resultant overall water flooding severity increased from 7.0 to 22.2 mV/min. Because the pressure, air stoichiometry, and relative humidity (100% RH) were fixed during measurement, the water content in the air at higher temperatures would have been larger than that at lower temperatures. This higher water content could make removal of water droplets more difficult, leading to more severe water flooding at the cathode.

### Effect of GDL Teflon Loading on Water Flooding

Different Teflon loadings on the gas diffusion layer were also tested to investigate their effects on the water flooding. Figure 7 shows two typical cell voltage–time curves at two Teflon loadings. It can be seen that a 5 wt% Teflon loading yielded much heavier water flooding than a 20 wt% Teflon loading. It is well known that Teflon is an effective water repelling agent due to its surface hydrophobicity. When it forms a thin film on the carbon fiber matrix of the GDL, the latter will become highly hydrophobic, facilitating water removal. Therefore, increasing the GDL's Teflon loading results in less water flooding. Raising the GDL's Teflon loading should thus be one of the most effective ways to reduce

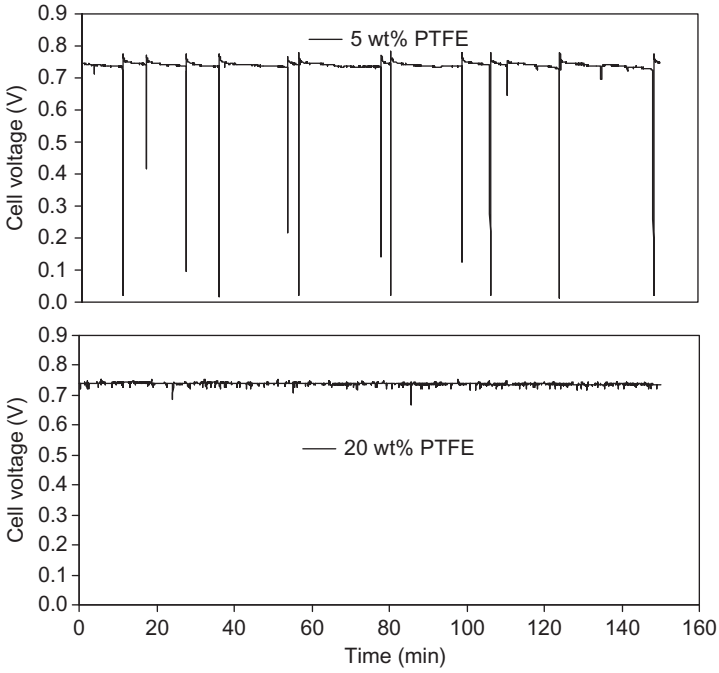


**Figure 7** Teflon (PTFE) loading affected fuel cell voltage as a function of time at a current density of 0.5 A/cm$^2$. The depth and width of the channel were both 1.0 mm. The fuel cell had a flow field design with triple serpentine flow channels. MEA area: 50 cm$^2$. Operating conditions: 80°C, 100% RH, 3.04 atm, $H_{2,ST} = 1.5$, $Air_{ST} = 2.0$.

water flooding. Note, however, that the Teflon loading should not be too high, otherwise it will considerably reduce GDL's conductivity. In practice, the optimal Teflon loading is around ~ 20–25 wt%.

## Effect of Flow Field Channel on Water Flooding

It has previously been recognized that the flowfield design could have a strong effect on water flooding (Li et al. 2007; Owejan et al. 2007; Shimpalee et al. 2006; Xu and Zhao 2007). In this paper, four serpentine flow channel design configurations were fabricated to investigate their effects on water flooding and concomitant fuel cell performance. Two kinds of flow channel patterns were designed: one had triple parallel serpentine flow channels with a channel width of 1.0 mm, and the other had single serpentine flow channels. The single serpentine flow channel design had three different channel widths: 1.0, 1.2, and 1.4 mm. All flow channel depths were 1.0 mm.

In terms of the fuel cell's steady-state performance, Figure 8 shows the polarization curves for these four flowfield designs. It can be seen that among the four curves, the fuel cell with a triple channel flowfield design gives the best steady-state performance. Unfortunately, as shown in Table 5, this triple parallel serpentine flow channel design showed the most severe water flooding. From Table 5 it can also be seen that for designs with single serpentine flow channel, the severity of water flooding increased with increasing channel width. The same trends were also observed at other current densities such as

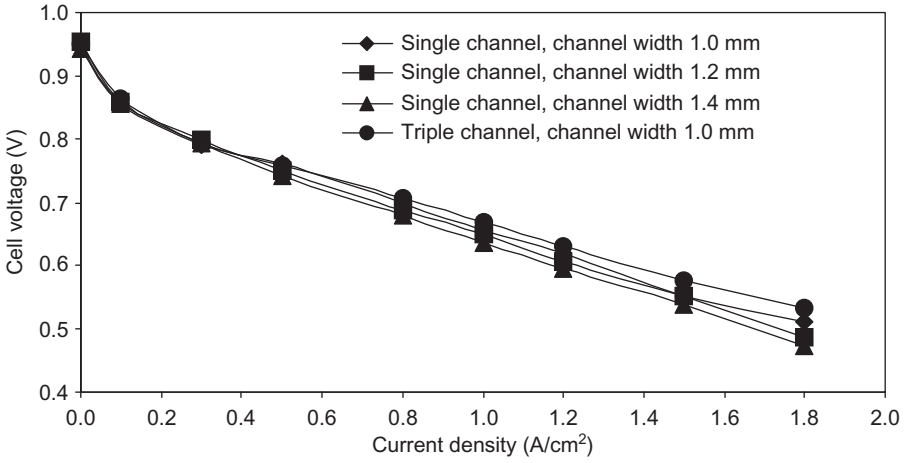


**Figure 8** Fuel cell performance with different flowfield designs for both anode and cathode. The depth and land width of all flow channels were 1.0 mm. MEA: 50 $cm^2$. GDL Teflon loading: 20 wt%. Operating conditions: 80°C, 100% RH, 3.04 atm, $H_{2,ST} = 1.5$, $Air_{ST} = 2.0$.

**Table 5** Water flooding severity at 0.5 $A/cm^2$ with different flowfield designs.

| Flow channel | $N_{wf}$ ($min^{-1}$) | $\Delta V_{wf}^{ave}$ (mV) | $\Psi_{wf}$ (mV/min) |
|---|---|---|---|
| Single channel, channel width 1.0 mm | 0.51 | 12.6 | 6.4 |
| Single channel, channel width 1.2 mm | 1.41 | 9.4 | 13.3 |
| Single channel, channel width 1.4 mm | 1.15 | 13.0 | 14.9 |
| Triple channel, channel width 1.0 mm | 0.73 | 30.3 | 22.2 |

*Note*. The depth and land width for all flow channels were 1.0 mm. MEA: 50 $cm^2$. GDL Teflon loading: 20 wt%. Operating conditions: 80°C, 100% RH, 3.04 atm, $H_{2,ST} = 1.5$, $Air_{ST} = 2.0$.

0.2 and 1.0 $A/cm^2$ (not shown here). This could be attributed to the decrease in air pressure drop at the cathode when channel width increased, as shown in Figure 9. For example, pressure drops of 0.17, 0.21, and 0.26 atm were recorded for channel widths of 1.0, 1.2, and 1.4 mm, respectively. The pressure drop for the triple serpentine channel flowfield was much lower (about one third) than the drop for the single serpentine channel flowfield with the same channel width, and even lower than that of channel with a 1.4 mm width. This is because the length of the gas pathway in the triple channel design is only one third of that in the single channel design. The higher pressure drop across the fuel cell channel aided in water removal, leading to less severe water flooding. However, as shown in Figure 8, the triple serpentine flow channel design showed the best performance. This can be ascribed to the shorter gas transport length, which facilitates more uniform distribution of the local oxygen concentration, temperature, water, and current (Shimpalee et al. 2006), leading to a better fuel cell stead-state performance.

## CONCLUSIONS

In this study, membrane electrode assemblies (MEAs) were constructed using catalyst-coated-membranes (CCMs) for fuel cell performance tests. Water flooding was

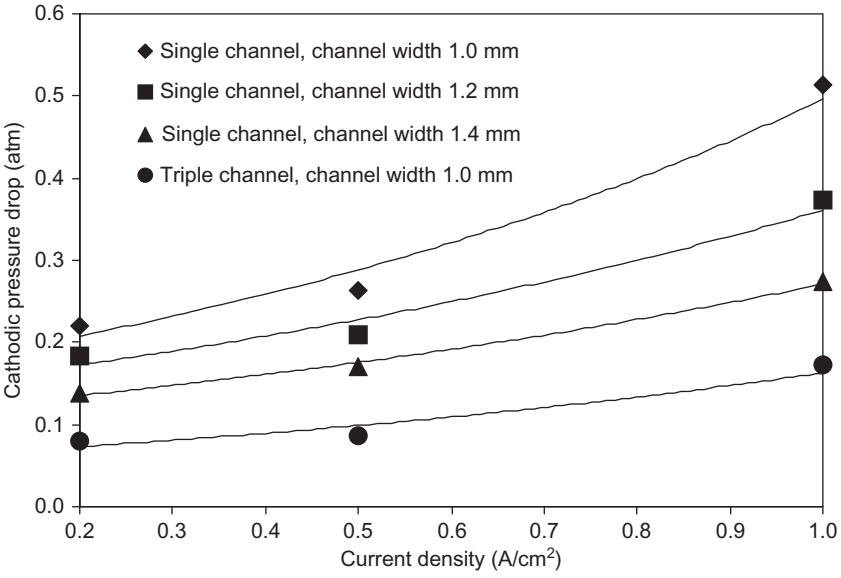


**Figure 9** Air pressure drops at cathode as a function of current density with different flow channels on flowfield plates. The depth and land width of all flow channels were 1.0 mm. MEA: 50 $cm^2$. GDL Teflon loading: 20 wt%. Operating conditions: 80°C, 100% RH, 3.04 atm, $H_{2,ST} = 1.5$, $Air_{ST} = 2.0$.



frequently observed when using such CCM-based MEAs in PEM fuel cell tests and operations. In order to quantitatively describe water flooding, a water flooding severity was defined in this paper.

Two major fuel cell hardware variations—flowfield design and Teflon loading of the gas diffusion layer—were tested to explore their effects on the water flooding. With respect to flowfield design, two kinds of flow channel patterns were evaluated: one had triple parallel serpentine flow channels and the other had single serpentine flow channels. The flowfield with triple serpentine flow channels showed heavier water flooding than of the flowfields with single serpentine flow channels. As for GDL Teflon loading effect, increasing the Teflon loading effectively reduced water flooding.

Several fuel cell operation conditions, namely air stoichiometry, current density, relative humidity, backpressure, and temperature, were also tested to identify their effects on water flooding. It was observed that the water flooding severity could be increased by decreasing the air stoichiometry and increasing the temperature, RH, backpressure, and current density. Among these operation conditions, both air stoichiometry (or air flow rate) and RH played the most important roles in reducing water flooding. However, during practical fuel cell operation, increasing the air stoichiometry will increase the system parasitic loss, and decreasing the RH will reduce the fuel cell performance. Therefore, reduction of water flooding also requires optimization of fuel cell operation conditions.

## ACKNOWLEDGMENTS

The authors gratefully acknowledge financial support from the National Research Council Canada's Institute for Fuel Cell Innovation (NRC-IFCI). In addition, the excellent assistance of Dr. Yanghua

Tang, Mr. Tom Vanderhoek, Mr. Kevin Berera, and Mr. Andrew Mattie in the design and fabrication of the flowfields is appreciated. The authors would also like to thank Professor Zhenxi Jiang, a Visiting Researcher at NRC-IFCI from Zheng Zhou University (China), for his help in the mathematical calculation of water flooding severity.

## REFERENCES

Barbir, F., H. Gorgun, and X. Wang. 2005. Relationship between pressure drop and cell resistance as a diagnostic tool for PEM fuel cells. *Journal of Power Sources* 141: 96–101.

Benziger, J. B., T. Whitaker, E. Kimball, and I. G. Kevrekidis. 2007. Liquid water transport in PEM fuel cells. *ECS Transactions* 12: 67–79.

Canut, J.-M. L., R. M. Abouatallah, and D. A. Harrington. 2006. Detection of membrane drying, fuel cell flooding, and anode catalyst poisoning on PEMFC stacks by electrochemical impedance spectroscopy. *Journal of the Electrochemical Society* 153: A857–A864.

Haile, S. M., D. A. Boysen, C. R. I. Chisholm, and R. B. Merle. 2001. Solid acids as fuel cell electrolytes. *Nature* 410: 910–913.

Hakenjos, A., H. Muenter, U. Wittstadt, and C. Hebling. 2004. A PEM fuel cell for combined measurement of current and temperature distribution, and flow field flooding. *Journal of Power Sources* 131: 213–216.

He, W., G. Lin, and T. V. Nguyen. 2003. Diagnostic tool to detect electrode flooding in proton-exchange-membrane fuel cells. *AIChE Journal* 49: 3221–3228.

Ihonen, J., M. Mikkola, and G. Lindbergh. 2004. Flooding of gas diffusion backing in PEFCs. *Journal of the Electrochemical Society* 151: A1152–A1161.

Larminie, J., and A. Dicks. 2001. *Fuel cell systems explained*, 1st ed. London: John Wiley & Sons Ltd.

Le, A. D., and B. Zhou. 2009. Fundamental understanding of liquid water effects on the performance of a PEMFC with serpentine-parallel channels. *Electrochimica Acta* 54: 2137–2154.

Li, H., Y. Tang, Z. Wang, Z. Shi, S. Wu, D. Song, J. Zhang, K. Fatih, J. Zhang, H. Wang, Z. Liu, R. Abouatallah, and A. Mazza. 2008. A review of water flooding issues in the proton exchange membrane fuel cell. *Journal of Power Sources* 178: 103–117.

Li, X., I. Sabir, and J. Park. 2007. A flow channel design procedure for PEM fuel cells with effective water removal. *Journal of Power Sources* 163: 933–942.

McKay, D. A., J. B. Siegel, W. Ott, and A. G. Stefanopoulou. 2008. Parameterization and prediction of temporal fuel cell voltage behavior during flooding and drying conditions. *Journal of Power Sources* 178: 207–222.

Meng, H., and C.-Y. Wang. 2005. Model of two-phase flow and flooding dynamics in polymer electrolyte fuel cells. *Journal of the Electrochemical Society* 152: A1733–A1741.

Owejan, J. P., T. A. Trabold, D. L. Jacobson, M. Arif, and S. G. Kandlikar. 2007. Effects of flow field and diffusion layer properties on water accumulation in a PEM fuel cell. *International Journal of Hydrogen Energy* 32: 4489–4502.

Park, Y. H., and J. A. Caton. 2008. Monitoring an electrode flooding through the back pressure in a proton exchange membrane (PEM) fuel cell. *International Journal of Green Energy* 5: 347–359.

Patel, S., A. S. Bansode, T. Sundararajan, and S. K. Das. 2008. The performance analysis of a multi-duct proton exchange membrane fuel cell cathode. *International Journal of Green Energy* 5: 35–54.

Shimpalee, S., S. Greenway, and J. W. Van Zee. 2006. The impact of channel path length on PEMFC flow-field design. *Journal of Power Sources* 160: 398–406.

Spernjak, D., A. K. Prasad, and S. G. Advani. 2007. Experimental investigation of liquid water formation and transport in a transparent single-serpentine PEM fuel cell. *Journal of Power Sources* 170: 334–344.

Steele, B. C. H., and A. Heinzel. 2001. Materials for fuel-cell technologies. *Nature* 414: 345–352.

Tang, Y., J. Zhang, C. Song, H. Liu, J. Zhang, H. Wang, S. Mackinnon, T. Peckham, J. Li, S. McDermid, and P. Kozak. 2006. Temperature dependent performance and in situ AC impedance of high-temperature PEM fuel cells using the Nafion-112 membrane. *Journal of The Electrochemical Society* 153: A2036–A2043.

Tüber, K., D. Pócza, and C. Hebling. 2003. Visualization of water buildup in the cathode of a transparent PEM fuel cell. *Journal of Power Sources* 124: 403–414.

Wang, X.-D., Y.-Y. Duan, W.-M. Yan, and F.-B. Weng. 2008. Effect of humidity of reactants on the cell performance of PEM fuel cells with parallel and interdigitated flow field designs. *Journal of Power Sources* 176: 247–258.

Wang, Z. H., C. Y. Wang, and K. S. Chen. 2001. Two-phase flow and transport in the air cathode of proton exchange membrane fuel cells. *Journal of Power Sources* 94: 40–50.

Weng, F.-B., A. Su, and C.-Y. Hsu. 2007. The study of the effect of gas stoichiometric flow rate on the channel flooding and performance in a transparent fuel cell. *International Journal of Hydrogen Energy* 32: 666–676.

Xu, C., and T. S. Zhao. 2007. A new flow field design for polymer electrolyte-based fuel cells. *Electrochemistry Communications* 9: 497–503.

Yang, X. G., F. Y. Zhang, A. L. Lubawy, and C. Y. Wang. 2004. Visualization of liquid water transport in a PEFC. *Electrochemical and Solid-State Letters* 7: A408–A411.

Yuan, J., and B. Sundén. 2004. Numerical analysis of heat transfer and gas flow in PEM fuel cell ducts by a generalized extended darcy model. *International Journal of Green Energy* 1: 47–63.